A comparison of PET imaging characteristics of various copper radioisotopes

Heather Ann Williams[1, 2], Simon Robinson[1], Peter Julyan[1], Jamal Zweit[2, 3], David Hastings[1]

[1] Christie Hospital NHS Trust, North Western Medical Physics, Wilmslow Road, Manchester, M20 4BX, United Kingdom
[2] Department of Instrumentation and Analytical Science, University of Manchester Institute of Science and Technology, Manchester, United Kingdom
[3] Radiochemical Targeting and Imaging, Paterson Institute for Cancer Research, Manchester, United Kingdom

Received: 14 April 2005 / Accepted: 4 July 2005 / Published online: 29 October 2005

Abstract. *Purpose:* PET radiotracers which incorporate longer-lived radionuclides enable biological processes to be studied over many hours, at centres remote from a cyclotron. This paper examines the radioisotope characteristics, imaging performance, radiation dosimetry and production modes of the four copper radioisotopes, ^{60}Cu, ^{61}Cu, ^{62}Cu and ^{64}Cu, to assess their merits for different PET imaging applications.
Methods: Spatial resolution, sensitivity, scatter fraction and noise-equivalent count rate (NEC) are predicted for ^{60}Cu, ^{61}Cu, ^{62}Cu and ^{64}Cu using a model incorporating radionuclide decay properties and scanner parameters for the GE Advance scanner. Dosimetry for ^{60}Cu, ^{61}Cu and ^{64}Cu is performed using the MIRD model and published biodistribution data for copper(II) pyruvaldehyde bis(N^4-methyl)thiosemicarbazone (Cu-PTSM).
Results: ^{60}Cu and ^{62}Cu are characterised by shorter half-lives and higher sensitivity and NEC, making them more suitable for studying the faster kinetics of small molecules, such as Cu-PTSM. ^{61}Cu and ^{64}Cu have longer half-lives, enabling studies of the slower kinetics of cells and peptides and prolonged imaging to compensate for lower sensitivity, together with better spatial resolution, which partially compensates for loss of image contrast. ^{61}Cu-PTSM and ^{64}Cu-PTSM are associated with radiation doses similar to [^{18}F]-fluorodeoxyglucose, whilst the doses for ^{60}Cu-PTSM and ^{62}Cu-PTSM are lower and more comparable with $H_2{}^{15}O$.
Conclusion: The physical and radiochemical characteristics of the four copper isotopes make each more suited to some imaging tasks than others. The results presented here assist in selecting the preferred radioisotope for a given imaging application, and illustrate a strategy which can be extended to the majority of novel PET tracers.

Heather Ann Williams (✉)
Department of Instrumentation and Analytical Science,
University of Manchester Institute of Science and Technology,
Manchester, United Kingdom
e-mail: hwilliams@physics.org

Keywords: Dosimetry – Positron emission tomography – Copper – Radioactive isotopes – Cu-PTSM

Eur J Nucl Med Mol Imaging (2005) 32:1473–1480
DOI 10.1007/s00259-005-1906-9

Introduction

Positron emission tomography (PET) has been developed around the positron-emitting isotopes of biologically important elements, carbon, oxygen and nitrogen (^{11}C, ^{15}O, and ^{13}N), which enable PET imaging to characterise the biodistributions of a wide range of small molecules. However, the very short half-lives of these radionuclides (20 min for ^{11}C, 2 min for ^{15}O, and 10 min for ^{13}N) preclude their use for the study of prolonged biological processes involving, for example, protein and peptide interactions with their cellular targets. Working with such short-lived radionuclides also means that an on-site cyclotron is essential. PET radiotracers based on longer-lived radionuclides with higher atomic numbers allow the study of physiological processes over periods of many hours or days, and make it possible to carry out PET imaging at centres remote from a cyclotron. Molecular PET imaging involves the study of biological pathways at the molecular and cellular level, and many of the PET radiotracers and radioligands used to target these processes will be developed using halogen and metal PET radionuclides [1–4].

^{18}F is by far the most commonly used of the longer-lived PET radionuclides, with a half-life of 110 min which allows imaging up to several hours after production. ^{18}F has been widely used for tumour imaging with FDG ([^{18}F]-fluorodeoxyglucose), and is also the PET nuclide most frequently investigated in the development of novel radiotracers and radioligands [2, 5].

Many of the other positron-emitting radionuclides with higher atomic numbers and longer half-lives have been investigated for both imaging and therapeutic purposes [6]

These include the halogens, ^{124}I, ^{120}I, ^{76}Br, and a number of metal radionuclides. The radio-coppers have attracted considerable attention [7] because they include isotopes which, due to their emission properties, offer themselves as agents of both diagnostic imaging (^{60}Cu, ^{61}Cu, ^{62}Cu and ^{64}Cu) and in vivo targeted radiation therapy (^{64}Cu and ^{67}Cu) [1, 8–13]. The properties and availability of these radioisotopes affect the exact applications in which they can be employed.

In this work, we examine the merits of the four copper radioisotopes, ^{60}Cu, ^{61}Cu, ^{62}Cu and ^{64}Cu, for imaging by PET, taking into account:

1. The effect of the radioactive emission characteristics on imaging performance
2. The impact of the radioactive decay properties on patient radiation dose
3. Cyclotron production and availability
4. The impact of (a) and (b) on the design of imaging methodology

Previously reported data from our group [14] are reviewed and combined with original results on imaging performance for ^{60}Cu and ^{61}Cu, where PET scanner performance is predicted from radionuclide decay properties and scanner parameters using our model [15]. The model combines the decay characteristics of a given PET radionuclide with the geometry and detection behaviours of the GE Advance PET scanner [16] to predict spatial resolution, sensitivity, scatter fraction and noise-equivalent count rate measures obtained under NEMA NU-2 1994 test conditions [17]. Radiation dosimetry estimates for ^{60}Cu, ^{61}Cu and ^{64}Cu are presented and compared with published data for ^{62}Cu. The impact of these issues is explored in the context of the perfusion radiotracer, copper(II) pyruvaldehyde bis(N^4-methyl)thiosemicarbazone (Cu-PTSM) [18].

Effect of the radioactive emission characteristics on imaging performance

Decay characteristics

The decay characteristics and emissions pertinent to PET imaging are summarised in Table 1 for the copper radioisotopes. For comparison, ^{15}O and ^{18}F are also included.

Spatial resolution

The positron range in tissue, prior to annihilation with an electron, increases with positron energy. The PET imaging process assumes that the annihilation lies along a line of response defined by the coincident photon pair, so that the annihilation registers the location of the radiation source. For a larger positron range there will be a greater discrepancy between the true and the assumed location of the positron emitter, leading to a degradation or blurring in spatial resolution. Investigations into the magnitude of this effect [24, 25] show that the relatively low positron energy of ^{18}F produces an insignificant resolution blurring of approximately 0.1 mm. This effect becomes more prominent for medium- to high-energy positron emitters such as ^{15}O, ^{82}Rb, ^{76}Br and the copper isotopes ^{60}Cu, ^{61}Cu and ^{62}Cu. We have demonstrated the effect of this resolution blurring on spatial resolution for the copper isotopes using our theoretical model, as shown in Table 2.

The severity of the blurring effect increases with positron energy, as demonstrated graphically in Fig. 1a, with the tangential spatial resolution increasing from 4.7 mm for ^{18}F to 7.2 mm for ^{62}Cu. The spatial resolution realised in the clinical setting is typically poorer than that measured under NU-2 1994 test conditions, as additional smoothing

Table 1. Key emissions for ^{60}Cu, ^{61}Cu, ^{62}Cu, ^{64}Cu, ^{15}O and ^{18}F. For β^+, energy=average of end-point energies, weighted by intensity

Nuclide	Half-life (min)	Radiation	Energy (keV)	Intensity (%)	Reference
^{60}Cu	23.4	β^+	2940	92	[19]
		γ	511	183	
			467	4	
			826	22	
			1332	88	
^{61}Cu	204.5	β^+	1159	62	[20]
		γ	511	123	
			283	12	
			589	1	
			656	11	
^{62}Cu	9.7	β^+	2925	93	[21]
		γ	511	155	
^{64}Cu	761.9	β^+	657	17	[22]
		γ	511	35	
			1346	1	
^{15}O	2.03	β^+	1723	100	[21]
		γ	511	200	
^{18}F	109.8	β^+	635	97	[23]
		γ	511	194	

Table 2. Imaging performance for the copper radioisotopes compared with ^{18}F and ^{15}O, for this centre's GE Advance scanner in 2D mode. ^{18}F values are measured; others are predicted using the methods of Robinson [15]. Spatial resolution, scatter fraction and sensitivity are derived according to the measurement principles of the NEMA NU-2 1994 standard [17]

Nuclide	Positron energy, weighted average of max (keV)	Positron decay fraction	Spatial resolution, centre of field of view (mm)		Scatter fraction (%)	Sensitivity (cps/Bq/ml)
			Tangential	Radial		
^{64}Cu	657	0.17	4.7	5.0	10.0	0.98
^{61}Cu	1159	0.62	5.1	5.4	11.0	3.43
^{60}Cu	2194	0.92	6.3	6.6	10.8	5.23
^{62}Cu	2925	0.97	7.2	7.4	10.0	5.50
^{15}O	1723	1.00	5.8	6.0	10.0	5.62
^{18}F	635	0.97	4.7	5.0	10.0	5.44

is used routinely in image reconstruction and the tissues of interest are not generally at the centre of the field of view.

Sensitivity, scatter fraction and noise-equivalent count rate

The dominant effect on sensitivity and count rate is the positron decay fraction, which directly affects the rate of true coincidences as a lower positron decay fraction results in fewer annihilation events per MBq. There are additional, smaller effects arising from associated gamma rays, emitted promptly as the daughter nucleus de-excites during the electron capture or positron emission process. These associated gammas may be emitted at several energies and some may be detected within the coincidence energy window of the scanner (300–650 keV), in addition to the pairs of annihilation gammas. Detection of associated gammas may reduce the coincidence count rate performance in one of three ways:

1. Triple events: the associated gamma is detected simultaneously with an annihilation pair, causing a triple event which the GE Advance rejects, reducing sensitivity
2. Additional random events: an annihilation gamma and an associated gamma from a separate decay, or two separate associated gamma rays, are detected in coincidence
3. Additional scatter-like events: one of a pair of annihilation gammas is detected in coincidence with an associated gamma ray from the same decay

The impact of the above effects on sensitivity and measured scatter fraction is shown in Table 2. The sensitivity values for ^{60}Cu, ^{62}Cu and ^{15}O are similar to that for ^{18}F, primarily because they have positron decay fractions close to unity. In contrast, the sensitivity is

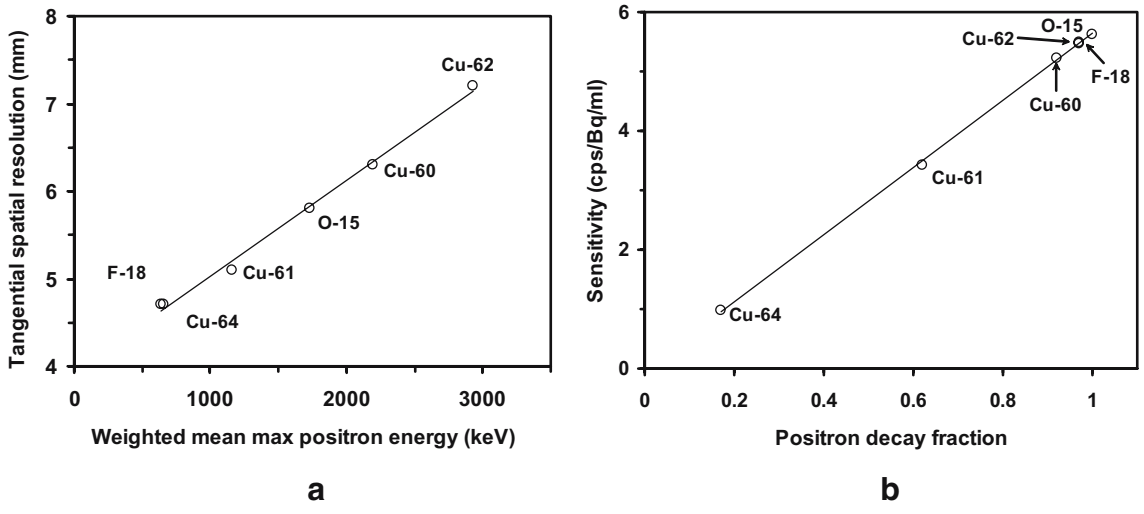

Fig. 1. a Variation of tangential spatial resolution with positron energy. **b** Variation of sensitivity with positron decay fraction. ^{18}F values were measured; values for the copper isotopes and ^{15}O were derived using Robinson's model [15]

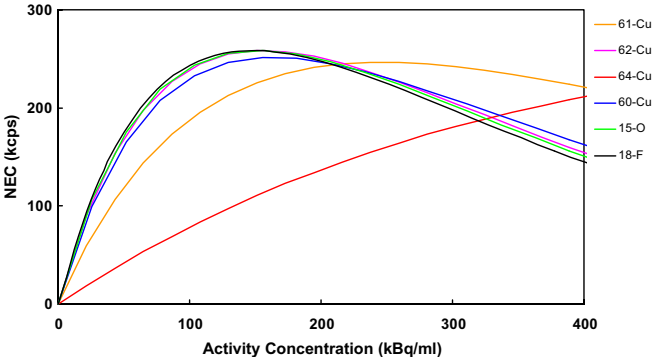

Fig. 2. Predicted variation of NEC rate with activity concentration for ^{60}Cu, ^{61}Cu, ^{62}Cu, ^{64}Cu and ^{15}O, compared with a fit to measured data for ^{18}F. Data were derived using the model of Robinson [15]

reduced for ^{61}Cu and more considerably so for ^{64}Cu. The observed relationship between sensitivity and positron decay fraction is shown in Fig. 1b. The scatter fractions are not significantly affected, all being similar to the 10% value for ^{18}F. The slightly higher scatter fractions for ^{60}Cu and ^{61}Cu result from the contributions of the associated gammas.

The variation of noise equivalent count rate (NEC) with activity concentration provides a more comprehensive assessment of the impact on imaging performance of the decay characteristics and consequent effects. NEC takes into account the relative contributions of the rates of true (T), random (R) and scattered (S) coincidences, and is directly related to signal to noise ratio [26]. NEC=$T/(1+S/T+2k_0R/T)$, where k_0 is the proportion of the projection covered by the object. Using our model, NEC curves for ^{60}Cu, ^{61}Cu, ^{62}Cu, ^{64}Cu and ^{15}O have been determined for a GE Advance scanner in 2D mode, as shown in Fig. 2.

For all the nuclides shown, the NEC curves demonstrate an initial rise in total and scattered event rates in proportion to activity, which departs from linearity at approximately 20 kBq/ml as the randoms fraction becomes increasingly significant, and eventually turns over due to deadtime effects. The magnitudes of the curve gradients are primarily in proportion to the positron decay fraction. The peak NEC (and hence, peak signal to noise ratio) occurs at a lower activity concentration for nuclides associated with a higher sensitivity measurement; this is approximately 150 kBq/ml for ^{62}Cu, ^{15}O and ^{18}F, 240 kBq/ml for ^{61}Cu and 820 kBq/ml for ^{64}Cu. The peak height for ^{60}Cu is slightly lower, due to coincident detection of direct and scattered associated gammas increasing the scatter and random contributions.

Dosimetric considerations

When performing radionuclide imaging studies of humans, it is necessary to strike a balance between administering enough activity to achieve high-quality image data and minimising radiation dose. The radiation dose from an administered radiotracer is dependent upon the radionuclide half-life and emission characteristics, and the biodistribution of the radiotracer compound. If a particular compound is labelled with different radionuclides, the radiation dose will vary according to the properties of the radionuclide.

Of the copper isotopes, ^{62}Cu has been most extensively used for imaging as a radiolabel for the perfusion agent, PTSM. We have used published ^{62}Cu-PTSM biodistribution data [27] to calculate the radiation doses for PTSM labelled with the other copper radioisotopes ^{60}Cu, ^{61}Cu, and ^{64}Cu. Radioactive decay data were obtained from tables of isotopes [28], and the calculations performed according to the MIRD (Medical Internal Radiation Dose) schema [29] using the software package MIRDOSE3 (Oakridge Associated Universities, Oak Ridge, TN) and S-factors determined by Stabin [personal communication, 2001]. The published work shows that Cu accumulates slowly in the liver over the hour following injection [27], so our analysis estimated the residence time in liver from the maximum accumulated activity and radioactive half-life. In vivo studies over a longer time period would be necessary to validate this assumption, as it may otherwise lead to an underestimation of the patient dose.

Table 3 shows the calculated effective and critical organ doses for PTSM labelled with each of the copper isotopes, together with values for $H_2{}^{15}O$ and ^{18}FDG. ^{60}Cu-, ^{61}Cu- and ^{64}Cu-PTSM result in higher effective doses than ^{62}Cu-PTSM. The radiation dose associated with ^{62}Cu-PTSM is of the same order as that for $H_2{}^{15}O$, while ^{61}Cu-PTSM is comparable with that for ^{18}FDG at 1.9 mSv/100 MBq, and ^{64}Cu-PTSM gives the highest effective dose of 3.8 mSv/100 MBq. It is apparent that the higher doses from ^{60}Cu, ^{61}Cu and ^{64}Cu are primarily due to their longer half-lives rather than to the intensity of their positron

Table 3. Calculated radiation doses for Cu-PTSM labelled with ^{60} Cu, ^{6} Cu and ^{64} Cu together with previously published values for ^{62} Cu-PTSM [27]. Values are also shown for ^{18} FDG and $H_2{}^{15}O$ for comparison. Physical half-lives and positron decay fractions shown from Table 2 are shown for ease of reference

Tracer	Physical half-life (min)	Positron decay fraction	Effective dose per 100 MBq (mSv)	Critical organ	Critical organ dose per 100 MBq (mGy)
^{62} Cu-PTSM	9.7	0.92	0.36	Liver	2.4
^{60} Cu-PTSM	23.4	0.17	1.1	Liver	6.1
^{61} Cu-PTSM	204.5	0.62	2.5	Liver	16
^{64} Cu-PTSM	761.9	0.97	3.8	Liver	20
[^{18} F]FDG	109.8	0.97	1.9 [30]	Bladder	7.3 [31]
$H_2{}^{15}O$	203	1.00	0.1 [30]	Heart	0.19 [30]

emissions. ^{64}Cu also has a negative beta decay branch (branching ratio=39%), and as β-particles have a relatively high linear energy transfer, they will contribute substantially to the higher radiation dose.

Production of copper isotopes and radiotracers

^{60}Cu, ^{61}Cu and ^{62}Cu are proton-rich nuclides and decay to their respective stable Ni isotopes through a combination of positron decay and electron capture processes. They can all be produced on a medical cyclotron using proton- or deuteron-induced reactions on enriched Ni targets (^{60}Ni, ^{61}Ni, ^{62}Ni). ^{62}Cu can also be produced indirectly through its parent ^{62}Zn in a ^{62}Zn/^{62}Cu generator system. ^{64}Cu is a highly unusual isotope because it decays by three processes, namely positron, electron capture and beta decays. This property allows either cyclotron or reactor production, with the latter route resulting in either low specific activity (n,γ) or high specific activity (n,p) products. Production data for the copper radionuclides are summarised in Table 4.

Extraction of each of the copper isotopes from the target takes approximately 45 minutes using ion exchange chromatography. For ^{62}Cu this is longer than four half-lives ($t_{1/2}$=9.7 min), and although very high yield is possible, this would necessitate initiating the radiochemistry with very high activity levels. Producing ^{62}Zn to make a ^{62}Zn/^{62}Cu generator system is the preferred option, reducing the levels of radioactivity that need to be manipulated and allowing ^{62}Cu to be eluted as required. Current ^{62}Zn/^{62}Cu generators can start with ^{62}Zn activities of 5–6 GBq, 93% of this activity being released as ^{62}Cu in the first 3.2 ml of eluate [38]. The 9.3-h half-life of ^{62}Zn enables a patient dose of ^{62}Cu-PTSM to be produced every 30 min for a full working day [40].

Copper isotopes can be used for labelling a wide range of compounds. Small molecules such as PTSM and copper (II) diacetyl bis(N^4-methyl)thiosemicarbazone (Cu-ATSM) [41] are tagged using metal-essential chemistry, and larger peptides and proteins labelled using cyclic polyamine chelators to enable metal coupling [1]. Metal-essential radiolabelling is rapid and efficient, as demonstrated by the synthesis of Cu-PTSM, which takes less than 5 min to complete and has an efficiency of more than 92% [38]. Of the copper isotopes considered here, only ^{62}Cu decays significantly during this period. Metal coupling radiolabelling is more complex and time consuming [1, 42, 43], and is better suited to isotopes with longer half-lives.

Impact on imaging methodology

Imaging characteristics

Decay characteristics impact on how a particular radionuclide can be used for an imaging investigation, although the magnitude of this impact will depend on the particular biochemical or physiological process under study, as well as on the biokinetics and specifics of trapping of the tracer compound.

The physical half-life dictates the time scale over which the tracer biodistribution can be visualised, which must be matched to the tracer kinetics and available imaging time. The biodistribution of smaller Cu-labelled tracer molecules, such as Cu-PTSM, is established rapidly and could therefore be studied adequately using the shorter-lived isotopes, ^{60}Cu ($t_{1/2}$=23.4 min) or ^{62}Cu ($t_{1/2}$=9.7 min). The

Table 4. Production data for copper radionuclides

	Isotope	Reaction	Incident beam energy (MeV)	Target enrichment (%)	Yield at EOB or recovery* (MBq/μAh or MBq/mg*)	Reference
Cyclotron	^{60}Cu	^{60}Ni(p,n)^{60}Cu	11	ND	370	[32]
	^{61}Cu	^{61}Ni(p,n)^{61}Cu	19	88.8	573[a]	[33]
	^{62}Cu	^{62}Ni(p,n)^{62}Cu	5–14	97.0	19800[a]	[34]
	^{64}Cu	^{64}Ni(p,n)^{64}Cu	12	94.8	243[b]	[35]
		^{64}Ni(d,2n)^{64}Cu	19	96.4	388[b]	[36]
		Zn(p,xn)^{64}Cu	ND	Natural Zn	67	[37]
Cyclotron + generator	^{62}Zn/^{62}Cu	^{63}Cu(p,2n)^{62}Zn	34, 47	Natural Cu	417[c]	[38]
		^{65}Cu(p,4n)^{62}Zn	58			
Reactor	^{64}Cu	^{64}Zn(n,p)^{64}Cu	1.8[e] (fast)	99.9	14.5[d]	[39]
		^{63}Cu(n,γ)^{64}Cu	ND	Natural Cu	ND	

ND data not available

[a]Predicted yield

[b]Maximum of results

[c]Total from three target positions

[d]Mean of results

[e]Approximate minimum neutron energy

physical half-life of ^{62}Cu restricts imaging to less than an hour following injection, but this has the advantage of allowing several repeat scans in quick succession, which can be used to evaluate response to a number of physiological or pharmacological stimuli [44]. The short half-life also offers the opportunity of dual tracer work, whereby a ^{62}Cu-labelled radiotracer study can be followed immediately by a different radiotracer study to provide complementary information on a related process. The longer-lived copper isotopes, ^{61}Cu ($t_{1/2}$=3.4 h) and ^{64}Cu ($t_{1/2}$=12.7 h), can be used to study the slower kinetics of larger proteins, such as peptides and antibodies, or cells.

As in any imaging situation, it is always necessary to maintain a balance between sensitivity and resolution. It can be seen from Fig. 1 that ^{18}F is close to the ideal case amongst the radioisotopes discussed here, having both high sensitivity (5.44 cps/Bq/ml) and the lowest spatial resolution (tangential=4.7 mm). For the copper isotopes and ^{15}O, one or both of these properties are compromised. For example, the spatial resolution of ^{64}Cu (radial=5.0 mm) is similar to that for ^{18}F because of their similar positron energies, but ^{64}Cu has the lowest sensitivity (0.98 cps/Bq/ml) due to its low positron decay fraction. These differences do not preclude successful imaging, but must be carefully taken into account when designing the imaging methodology. The higher sensitivities associated with ^{62}Cu and ^{60}Cu offer shorter data acquisition periods for the same administered activity. If ^{61}Cu and ^{64}Cu are deemed appropriate for other reasons, then longer acquisition times can compensate provided tracer kinetic information is not compromised and patient tolerability permits. It is also necessary to increase imaging times for isotopes which emit higher energy positrons and are consequently associated with poorer spatial resolution, in order to improve counting statistics and maintain lesion detectability. Simulations by Muellehner show that the number of detected events should be increased fourfold for each 2-mm increase in spatial resolution [45].

The activity at which image quality is optimised in terms of noise characteristics can be determined for a particular nuclide from the activity concentration at which the peak NEC value occurs. Although the concentrations at which the NEC curves in Fig. 2 peak are not reached in patient studies, the ordering of the NEC curves at lower concentrations can still be used as an indicator of relative image quality. These data are directly related to the positron decay fraction and measured sensitivity, but do not take spatial resolution into account.

For a given radionuclide, the trade-off between total counts and spatial resolution can be evaluated using a phantom which simulates the radiotracer biodistribution for a particular clinical application. Such phantom studies can also be used to evaluate various means of compensating for variations in spatial resolution, such as modification of the region of interest size used in image analysis [46, 47] or recovering the 'lost' resolution using advanced EM reconstruction algorithms [48].

Dosimetry

All studies resulting in a radiation dose to humans are subject to regulatory limitations on the levels of activity which can be administered. This can impose compromises on methodologies designed with the sole aim of optimising imaging characteristics, although in some cases it may be possible to justify the additional risk of radiation-induced disease or damage associated with a higher administered activity. One such example is the use of PET studies for evaluating the pharmacokinetics and pharmacodynamics of new anti-cancer agents in the terminally ill. Therefore, the choice of isotope need not depend solely on the information required from the imaging technique; rather, it may also depend on the nature of the clinical application. For tracers with slower kinetics, it may also be possible to compensate for a lower administered dose by extending the imaging period, providing this can be tolerated by the subject.

In the case of perfusion studies with Cu-PTSM, it can be seen from Table 3 that the use of ^{62}Cu-PTSM should be considered first to achieve the lowest possible radiation burden. However, as the concentration of radioactive Cu in tissue reaches a plateau approximately 5 min after injection [49] which is proportional to blood flow for all but the highest flow rates (>10 ml·min^{-1}·100 g) [50], measures of perfusion could still be obtained using ^{60}Cu, ^{61}Cu or ^{64}Cu if ^{62}Cu is not readily available.

Availability

The availability of particular copper isotopes is often the ultimate limiting factor in designing an imaging methodology. As is seen from Table 4, the availability of copper isotopes is dictated by the proximity of a reactor or a cyclotron to the investigational centre, and even the energy and composition of the cyclotron beam. In addition to the cyclotron, suitable facilities are required for the safe and efficient extraction of the radioisotope from the target. The ^{62}Zn/^{62}Cu generator is a practical solution for centres at some distance from laboratories with a reactor or cyclotron, although ^{64}Cu ($t_{1/2}$=12.7 h) can be shipped over considerable distances.

Conclusion

PET imaging is possible with all of the copper isotopes, ^{60}Cu, ^{61}Cu, ^{62}Cu and ^{64}Cu. Each has its own particular characteristics which make it more or less preferable for a given application.

The shorter half-lives and higher positron decay fractions of ^{60}Cu and ^{62}Cu make them suitable for characterising the faster kinetics of smaller tracer molecules, such as Cu-PTSM or Cu-ATSM. The longer half-lives of ^{61}Cu and ^{64}Cu are better suited to studying the slower kinetics of labelled peptides, antibodies and cells. Their longer half-

lives also permit an extended imaging period to compensate for the lower sensitivity associated with these isotopes, although the loss of image contrast due to poorer counting statistics is partially compensated by better spatial resolution. In the case of Cu-PSTM, ^{61}Cu and ^{64}Cu are associated with a radiation dose per unit activity of similar magnitude to that for ^{18}FDG. The radiation burden for ^{60}Cu-PTSM or ^{62}Cu-PTSM is considerably lower, and more comparable with that for $H_2{}^{15}O$.

The various characteristics and modes of production of ^{60}Cu, ^{61}Cu, ^{62}Cu and ^{64}Cu have been described here, including the imaging performance, radiation dosimetry and availability. Imaging performance and dosimetry results presented here make it possible to decide on the best imaging methodology for a given application using one of these radioisotopes. The strategy of relating isotope decay characteristics to imaging performance and radiation dosimetry is more widely applicable, being valuable in guiding labelling and imaging strategies for the majority of novel PET tracers.

Acknowledgements. The authors wish to thank Michael Stabin of Vanderbilt University (Nashville, USA) for ^{60}Cu, ^{61}Cu and ^{64}Cu S-factors, and Jeff Lacy of Proportional Technologies Inc. (Houston, USA) for clarifying the organ residence times for ^{62}Cu-PTSM.

The work detailed in this paper was carried out in compliance with current UK law.

References

1. Blower PJ, Lewis JS, Zweit J. Copper radionuclides and radiopharmaceuticals in nuclear medicine. Nucl Med Biol 1996;23:957–80
2. Gambhir SS. Molecular imaging of cancer with positron emission tomography. Nat Rev Cancer 2002;2:684–93
3. Jayson GC, Zweit J, Jackson A, Mulatero C, Julyan P, Ranson M, et al. Molecular imaging and biological evaluation of HuMV833 anti-VEGF antibody: implications for trial design of antiangiogenic antibodies. J Natl Cancer Inst 2002;94:1484–93
4. Reader AJ, Zweit J. Developments in whole-body molecular imaging of live subjects. Trends Pharmacol Sci 2001;22:604–7
5. Gambhir SS, Herschman HR, Cherry SR, Barrio JR, Satyamurthy N, Toyokuni T, et al. Imaging transgene expression with radionuclide imaging technologies. Neoplasia 2000;2:118–38
6. Zweit J. Radionuclides and carrier molecules for therapy. Phys Med Biol 1996;41:1905–14
7. Smith SV. Molecular imaging with copper-64. J Inorg Biochem 2004;98:1874–901
8. Anderson CJ, Dehdashti F, Cutler PD, Schwarz SW, Laforest R, Bass LA, et al. ^{64}Cu-TETA-octreotide as a PET imaging agent for patients with neuroendocrine tumours. J Nucl Med 2001; 42:213–21
9. Adonai N, Nguyen KN, Walsh J, Iyer M, Toyokuni T, Phelps ME, et al. Ex vivo cell labeling with ^{64}Cu-pyruvaldehydge-bis (*N*4-methylthiosemicarbazone) for imaging cell trafficking in mice with positron emission tomography. Proc Natl Acad Sci U S A 2002;99:3030–5
10. Dehdashti F, Grigsby PW, Mintun MA, Lewis JS, Siegel BA, Welch MJ. Assessing tumour hypoxia in cervical cancer by positron emission tomography with ^{60}Cu-ATSM: relationship to therapeutic response—a preliminary report. Int J Radiat Oncol Biol Phys 2003;55:1233–8
11. Lewis MR, Wang M, Axworthy DB, Theodore LJ, Mallett RW, Fritzberg AR, et al. In vivo evaluation of pretargeted ^{64}Cu for tumor imaging and therapy. J Nucl Med 2003;44:1284–92
12. Bischof Delaloye A, Delaloye B, Buchegger F, Vogel C-A, Gillet M, Mach J-P, et al. Comparison of copper-67-and iodine-125-labeled anti-CEA monoclonal antibody biodistribution in patients with colorectal tumours. J Nucl Med 1997;38:847–53
13. Grünberg J, Knogler K, Waibel R, Novak-Hofer I. High-yield production of recombinant antibody fragments in HEK-293 cells using sodium butyrate. Biotechniques 2003;34:968–72
14. Julyan PJ, Robinson S, Bailey J, Reader AJ, Marsland B, Kacperek A, et al. Performance of the GE advance PET scanner for non-pure positron emitters—prediction and validation using ^{124}I. J Nucl Med 2001;42 suppl:205P
15. Robinson S, Julyan PJ, Hastings DL, Zweit J. Performance of a block detector PET scanner in imaging non-pure positron emitters—modelling and experimental validation with ^{124}I. Phys Med Biol 2004;49:5505–28
16. DeGrado TR, Turkington TG, Williams JJ, Stearns CW, Hoffman JM, Coleman RE. Performance characteristics of a whole-body PET scanner. J Nucl Med 1994;35:1398–406
17. Karp JS, Daube-Witherspoon ME, Hoffman EJ, Lewellen TK, Links JM, Wong WH, et al. Performance standards in positron emission tomography. J Nucl Med 1991;12:2342–50
18. Green MA, Mathias CJ, Welch MJ, McGuire AH, Perry D, Fernandez-Rubio F, et al. Copper-62-labeled pyruvaldehyde bis (*N*4-methylthiosemicarbazonato)copper(II): synthesis and evaluation as a positron emission tomography tracer for cerebral and myocardial perfusion. J Nucl Med 1990;31:1989–96
19. King MM. Nuclear data sheets update for A=60. Nucl Data Sheets 1993;69:1–67
20. Bhat MR. Nuclear data sheets for A=61. Nucl Data Sheets 1999;88:417–532
21. Junde H, Singh B. Nuclear data sheets for A=62. Nucl Data Sheets 2000;91:317–422
22. Singh B. Nuclear data sheets for A=64. Nucl Data Sheets 1996;78:395–546
23. Tilley DR, Weller HR, Cheves CM, Chasteler RM. Energy levels of light nuclei A=18–19. Nucl Phys 1995;A595:1–170
24. Levin CS, Hoffman EJ. Calculation of positron range and its effect on the fundamental limit of positron emission tomography system spatial resolution. Phys Med Biol 1999;44:781–99
25. Derenzo SE, Hasigut RR, Fujiwara K. Precision Measurement of annihilation point spread distributions for medically important positron emitters. Positron annihilation. Sendai: The Japan Institute of Metals; 1979
26. Strother SC, Casey ME, Hoffman EJ. Measuring PET scanner sensitivity: relating countrates to image signal-to-noise ratios using noise equivalent counts. IEEE Trans Nucl Sci 1990; 37:783–8
27. Wallhaus TR, Lacy J, Whang J, Green MA, Nickles RJ, Stone CK. Human biodistribution and dosimetry of the PET perfusion agent copper-62-PTSM. J Nucl Med 1998;39:1958–64
28. Lederer CM, Shirley VS. Tables of the isotopes. 7th ed. New York: Wiley; 1978
29. Loevinger R, Budinger TF, Warson EE. MIRD primer for absorbed dose calculations: revised edition. New York: Society of Nuclear Medicine; 1991
30. ICRP [International Commission on Radiation Protection]. ICRP 80: Radiation dose to patients from radiopharmaceuticals (Addendum 2 to ICRP 53). Ann ICRP 1998;28:1–126
31. Hays MT, Watson EE, Thomas SR, Stabin M. MIRD dose estimate report no. 19: Radiation absorbed dose estimates from ^{18}F-FDG. J Nucl Med 2002;43:210–4
32. Martin CC, Oakes TR, Nickles RJ. Small cyclotron production of [Cu-60] for PET blood flow measurements. J Nucl Med 1990;31:815P

33. Szelecsényi F, Blessing G, Qaim SM. Excitation functions of proton induced nuclear reactions on enriched ^{61}Ni and ^{64}Ni: possibility of production of no-carrier-added ^{61}Cu and ^{64}Cu at a small cyclotron. Appl Radiat Isotopes 1993;44:575–80
34. Piel H, Qaim SM, Stöcklin G. Excitation functions of (p,xn)-reactions on natNi and highly enriched ^{62}Ni: possibility of production of medically important radioisotope ^{62}Cu at a small cyclotron. Radiochim Acta 1992;57:1–5
35. Obata A, Kasamatsu S, McCarthy DW, Welch MJ, Saji H, Yonekura Y, et al. Production of therapeutic quantities of ^{64}Cu using a 12 MeV cyclotron. Nucl Med Biol 2003;30:535–9
36. Zweit J, Smith AM, Downey S, Sharma HL. Excitation functions for deuteron induced reactions in natural nickel: production of no-carrier-added ^{64}Cu from enriched ^{64}Ni targets for positron emission tomography. Appl Radiat Isotopes 1991; 42:193–7
37. Smith SV, Waters DJ, Di Bartolo NM, Hocking R. Novel separation of ultra pure high specific activity Cu-64. J Label Compd Radiopharm 2003;46:S45
38. Zweit J, Goodall R, Cox M, Babich JW, Potter GA, Sharma HL, et al. Development of a high performance zinc-62/copper-62 radionuclide generator for positron emission tomography. Eur J Nucl Med 1992;19:418–25
39. Zinn KR, Chaudhuri TR, Cheng TP, Morris JS, Meyer WA Jr. Production of no-carrier-added ^{64}Cu from zinc metal irradiated under boron shielding. Cancer 1994;73:774–8
40. Haynes NG, Lacy JL, Nayak N, Martin CS, Dai D, Mathias CJ, et al. Performance of a ^{62}Zn/^{62}Cu generator in clinical trials of PET perfusion agent ^{62}Cu-PTSM. J Nucl Med 2000;41:309–14
41. Fujibayashi Y, Taniuchi H, Yonekura Y, Ohtani H, Konishi J, Yokoyama A. Copper-62-ATSM: a new hypoxia imaging agent with high membrane permeability and low redox potential. J Nucl Med 1997;38:1155–60
42. Anderson CJ, Pajeau TS, Edwards WB, Sherman EL, Rogers BE, Welch MJ. In vitro and in vivo evaluation of copper-64-octreotide conjugates. J Nucl Med 1995;36:2315–25
43. Anderson CJ, Connett JM, Schwarz SW, Rocque PA, Guo LW, Philpott GW, et al. Copper-64-labeled antibodies for PET imaging. J Nucl Med 1992;33:1685–91
44. Flower MA, Zweit J, Hall AD, Burke D, Davies MM, Dworkin MJ, et al. ^{62}Cu-PTSM and PET used for the assessment of angiotensin II-induced blood flow changes in patients with colorectal liver metastases. Eur J Nucl Med 2001;28:99–103
45. Muellehner, G. Effect of resolution improvement on required count density in ECT imaging: a computer simulation. Phys Med Biol 1985;30:163–73
46. Ribeiro MJ, Almeida P, Strul D, Ferreira N, Loc'h C, Brulon V, et al. Comparison of fluorine-18 and bromine-76 imaging in positron emission tomography. Eur J Nucl Med 1999;26:758–66
47. Williams HA, Julyan PJ. What you see ain't what you get: investigating concentration recovery in PET. Nucl Med Commun 2003;24:456
48. Reader AJ, Julyan PJ, Williams H, Hastings DL, Zweit J. EM algorithm system modeling by image-space techniques for PET reconstruction. IEEE Trans Nucl Sci 2003;50:1392–7
49. Okazawa H, Yonekura Y, Fujibayashi Y, Nishizawa S, Magata Y, Ishizu K, et al. Clinical application and quantitative evaluation of generator-produced copper-62-PTSM as a brain perfusion tracer for PET. J Nucl Med 1994;35:1910–5
50. Mathias CJ, Welch MJ, Raichle ME, Mintun MA, Lich LL, McGuire AH, et al. Evaluation of a potential generator-produced PET tracer for cerebral perfusion imaging: single-pass cerebral extraction measurements and imaging with radiolabeled Cu-PTSM. J Nucl Med 1990;31:351–9